

ICNTC E-CONFERENCE
INTERNATIONAL CONFERENCE ON NEW TRENDS IN CHEMISTRY

7th INTERNATIONAL CONFERENCE ON NEW TRENDS IN CHEMISTRY
25 - 26 SEPTEMBER 2021

7th ICNTC PROCEEDINGS BOOK

ICNTC E-CONFERENCE
INTERNATIONAL CONFERENCE ON NEW TRENDS IN CHEMISTRY

7th INTERNATIONAL CONFERENCE ON NEW TRENDS IN CHEMISTRY

25 – 26 SEPTEMBER 2021

<http://www.icntcconference.com/>

ICNTC E- Conference 2021

7th International Conference on New Trends in Chemistry

Published by the ICNTC Secretariat

Editor:

Assoc. Prof. Dr. Dolunay ŞAKAR DAŞDAN

ICNTC Secretariat

Büyükdere Cad. Ecza sok. Pol Center 4/1 Levent-İstanbul

E-mail: icntcconference@gmail.com

<http://www.icntcconference.com>

Conference organised in collaboration with Monre Academy

ISBN: 978-605-67476-8-7

Copyright @ 2021 ICNTC and Authors

All Rights Reserved

No part of the material protected by this copyright may be reproduced or utilized in any form or by any means electronic or mechanical, including photocopying , recording or by any storage or retrieval system, without written permission from the copyrights owners

SCIENTIFIC COMMITTEE

Prof. Dr. Janusz Stafiej,
Cardinal Stefan Wyszyński University, Warsaw, Poland

Assoc. Prof. Dr. Dolunay Sakar Dasdan,
Yıldız Technical University, Turkey
Conference Chair

PhD Dr. Habil. Agnieszka Kaczor,
Medical University of Lublin, Poland

PhD Dr. Habil. Agata Bartyzel,
University of Maria Curie-Skłodowska, Poland

PhD Dr. Habil. Daniel Ayuk Mbi Egbe,
Linz Institute for Organic Solar Cells, Austria

Dr. Eduardo V. Ludeña,
Escuela Superior Politécnica del Litoral Ecuador

Dr. Hatem M.A. Amin
Faculty of Chemistry and Biochemistry, Ruhr-University Bochum, Germany

Dr. Mauricio Heriberto Cornejo Martinez,
Escuela Superior Politécnica del Litoral Ecuador

PhD Pabitra Saha
RWTH Aachen University, Aachen, Germany

PhD Flavio Massignan
Eötvös Loránd University, Budapest, Hungary

ORGANIZATION COMMITTEE

Assoc. Prof. Dr. Dolunay Sakar Dasdan
Yıldız Technical University – Turkey
Conference Chair

Prof. Dr. Yelda Yalcin Gurkan
Namik Kemal University – Turkey
Chemistry Department

Dear Colleagues,

I am honoured to invite and send you this call for papers on behalf of Conference Organisation Board of “7th International Conference on New Trends in Chemistry”, to be held as based on Online Presentations dates between September 25-26, 2021

Limited number of Papers and Posters with the below mentioned topics will be accepted for our conference:

- Polymer Chemistry and Applications
- Pharmaceutical Chemistry
- Computational Chemistry
- Bio Chemistry
- Physical Chemistry
- Analytical Chemistry
- Inorganic Chemistry
- Organic Chemistry
- Material Chemistry
- Environmental Chemistry
- Food Chemistry

The selected papers which are presented as oral in the conference will be published in a international peer-reviewed journal which is scanned by SCOPUS as Q4. Each manuscript will have doi Numbers.

We kindly wait for your attendance to our online conference to be held on 25 –26th of September 2021,

All informations are available in conference web site. For more information please do not hesitate to contact us. info@icntconference.com

Respectfully Yours,

On Behalf of the Organization Committee of ICNTC Conference

Assoc. Prof. Dr. Dolunay SAKAR DASDAN
7th ICNTC 2021 | Conference Chair
Yıldız Technical University – Istanbul / Turkey
Chemistry Department

SCIENTIFIC PROGRAM

25 SEPTEMBER 2021 SATURDAY

Online access : with given username and password.

10:00 – 10:10

Welcome Speech : **Assoc. Prof. Dr. Dolunay SAKAR DASDAN** / Conference
Chair

Yildiz Technical University, Turkey

10:10 – 11:00

Keynote Speaker : **Dr. Hatem AMIN** / Cairo University, Egypt
Speech Title : **Oxygen Electrocatalysis at Metal Oxides and Sulfides:
From Fundamentals to Applications**

| | |
|----------------------|------------------|
| 11:00 – 11:15 | B R E A K |
|----------------------|------------------|

SESSION A

| SESSION CHAIR | Dr.Hatem AMIN | |
|--------------------------|--|---|
| TIME | PAPER TITLE | PRESENTER / CO AUTHOR |
| 11:15 – 11:30 | Powder Mixtures of β -Tricalcium Phosphate and Potassium Hydrosulfate Homogenized Under Mechanical Activation For Ceramics Preparation | Tatiana SAFRONOVA, Marat AKHMEDOV, Tatiana SHATALOVA, Snezhana TIKHONOVA, Gilyana KAZAKOVA, Maksim KAIMONOV, Alexander KNOTKO |
| 11:30 – 11:45 | Olive Leaf Extract and Potential of Transdermal Application | Hicran BELLUCCI, Ozlem DOGAN |
| 11:45 – 12:00 | Antioxidant Activity of <i>Rumex Patientia L.</i> Leaves and Analysis of Its Polyphenol Contents By Lc-Ms/Ms | Derya ALTINTAS, Yesim YESILOGLU |
| 12:00 – 12:15 | Theoretical and Experimental Photodegradation of Phosmet Via Oxidation Techniques in The Presence of Aqueous TiO ₂ Suspension | Bahar EREN, Yelda YALCIN GURKAN |

| | |
|-------------------------|--------------------|
| 12:15– 13:15 | LUNCH BREAK |
|-------------------------|--------------------|

25 SEPTEMBER 2021 SATURDAY

Online access : with given username and password

SESSION B

| SESSION CHAIR | Dr.Emel AKYOL | |
|------------------|--|---|
| TIME | PAPER TITLE | PRESENTER / CO AUTHOR |
| 13:15 – 13:30 | Determination of Some Metal Levels in Exotic Fruits by ICP-OES | Ayca KARASAKAL |
| 13:30 – 13:45 | Antibacterial Surface Properties of Polyester Fibers With Cu-Based Mof | Betul YENIDOGAN, Sennur DENIZ |
| 13:45 – 14:00 | Surface Modification of Zeolite and Kaolin with Different Silanization Agents | Cem OZEL, Cansu AKAT, Rasim ALASMANOV, Muhammet U. KAHVECI, Ceren EMIR, Sevil YUCEL |
| 14:00 – 14:15 | Gas Separation Properties of Mixed Matrix Membranes Prepared With Graphene Oxide | Sevgi CANCA, Sennur DENIZ |

| | |
|------------------|------------------|
| 14:15 – 14:30 | B R E A K |
|------------------|------------------|

SESSION C

| SESSION CHAIR | Dr.Sevil YÜCEL | |
|------------------|--|--|
| TIME | PAPER TITLE | PRESENTER / CO AUTHOR |
| 14:30 – 14:45 | Biodegradable Flexible PLA/PCL Films With Natamycin and Nanocellulose | Nudem KAHRAMAN, Sennur DENIZ |
| 14:45 – 15:00 | Photocatalytic Degradation of Methylene Blue By Nano-Titanium Dioxide Composites | Emel AKYOL, Guldeniz TONBUL |
| 15:00 – 15:15 | Colorimetric Method For Insulin Detection Using a New Magnetic Nanozyme | Burcu GOKCAL, Kadriye Özlem HAMALOGLU |
| 15:15 – 15:30 | Investigation of Controlled Drug Delivery of Ethyl Cellulose | Busra TURAN, Pelin DEMIRCIVI |

| | | |
|--------------------------|--|--|
| 15:30 – 15:45 | Preparation of Sulfonimide Functional Proton Conducting Polymers | Elif Busra CELEBI, Ferda HACIVELIOGLU |
| 15:45 – 16:00 | Synthesis and Characterisation of a Glutathione-Stransferase (hGSTP1-1) Single Nucleotide Polymorphs (Part II) | Sadhna MATHURA |
| 16:00 – 16:15 | B R E A K | |

25 SEPTEMBER 2021 SATURDAY

Online access : with given username and password

POSTER SESSION A

| SESSION CHAIR | Dr.Yelda YALÇIN GÜRKAN | 5 min oral presentation after that questions from participants |
|-----------------------------|---|--|
| TIME | PAPER TITLE | PRESENTER / CO AUTHOR |
| 16:15 16:45 | Preparation of Gelatin Coated Alginate Capsules | Gulzhan YERLAN, Bakyt TYUSSYUPOVA, Sagdat TAZHIBAYEVA, Kuanyshbek MUSABEKOV |
| | Synthesis and Characterization of Terpyridine Functional Cyclophosphazene | Elif Büşra ÇELEBİ, Halil DUYAR, Ferda HACIVELİOĞLU |
| | Investigation of Trace and Major Element Concentrations of Almond Milk by Using an Inductively Coupled Plasma Optical Emission Spectrometer | Ayca KARASAKAL |
| | Synthesis and Characterization of LDH Materials and Their Application in Wastewater Treatment | Abderrahmane HIRI, Achour DAKHOUCHE, Kamel NOUFEL Kamel NOUFEL |

26 SEPTEMBER 2021 SUNDAY

SESSION D

| SESSION CHAIR | Dr.Bahar Eren | |
|----------------------|---|-------------------------------------|
| TIME | PAPER TITLE | PRESENTER / CO AUTHOR |
| 09:30 - 09:45 | Determination of Human Papillomavirus-11 with Impedimetric CRISPR Biosensor | Zihni Onur UYGUN |
| 09:45 – 10:00 | Thermal Analysis and Isoconversional Kinetics Study of Thermal Decomposition of Polycyclohexene Oxide Polystyrene (PCHO-PSt) Comb-Shaped Polymer | Hacer DOLAS, Nasrettin GENLI |
| 10:00 – 10:15 | CRISPR-dCas9 Based Biosensor System for Detection of Sickle Cell Anemia | Hilmiye Deniz ERTUGRUL UYGUN |
| 10:15 – 10:30 | Phenol Containing Bodipy Functionalized Anderson Type Pom: Synthesis, Characterization and Photophysical Properties | Seda CETINDERE |
| 10:30 – 10:45 | Determination of Free Energy Difference Between Anomaly Solid-Liquid Phase Transitions of Silicon Using Pseudo-Supercritical Thermodynamic Path: A Molecular Dynamics Study | Chandan K DAS |
| 10:45- 11:00 | Investigation of Stability and Activity of Poly(ethylene-alt-maleic anhydride) Copolymer in Different pHs and Simulated Body Fluids | Dolunay ŞAKAR DAŞDAN |
| 11:00– 11:15 | B R E A K | |

26 SEPTEMBER 2021 SUNDAY

Online access : with given username and password

SESSION E

| SESSION CHAIR | Dr.Dolunay ŞAKAR DAŞDAN | |
|------------------|--|---|
| TIME | PAPER TITLE | PRESENTER / CO AUTHOR |
| 11:15 – 11:30 | Production And Characterization of Composite Scaffolds By Electrospinning Technique From Bioceramics Synthesized From Seashells | Sema Nur SAHIN , Erdi BULUS, Demet Sezgin MANSUROGLU, Bahadir BOZKURT, Aziz KORKUT, Yesim Muge SAHIN |
| 11:30 - 11:45 | New Approaches in Green Chemistry: Vaniline Based Imin Synthesis and Wound Dressing Production by Nanotechnology | Yeşim Müge SAHIN , Erdi BULUS, Demet Sezgin MANSUROGLU, Bahadir BOZKURT, Hatice Dilara SARAC, Funda OZKOK, Nihal ONUL, Tatyana TISHAKOVA, Gulru OZAY |
| 11:45 – 12:00 | Synthesis and Dielectrophoretic Alignment of Metal Oxide Nanowires for Applications in Diverse Devices | Raitis SONDORS , Davis GAVARS, Matiss RAMMA, Donats ERTS, Jana ANDZANE |
| 12:00 - 12:15 | The Biosphere Self-Organization Attractors Drive Perfect Order Homeostasis Reactions to Link Bioenergetic with Functionally Activate Oxygen and Carbon Dioxide Molecules | Aris KAKSIS |
| 12:15 – 12:30 | CLOSING CEREMONY | |

CONTENTS

| | |
|---|----|
| <u>1</u> -ANTIOXIDANT ACTIVITY of <i>RUMEX PATIENTIA</i> L. LEAVES and ANALYSIS of ITS POLYPHENOL CONTENTS by LC-MS/MS | |
| Derya ALTINTAS, Yesim YESILOGLU, | 13 |
| <u>2</u> -Determination of Free Energy Difference between Anomaly Solid-Liquid Phase Transitions of Silicon using Pseudo-supercritical Thermodynamic Path: A Molecular Dynamics Study | |
| Chandan K Das..... | 17 |
| <u>3</u> -PHENOL CONTAINING BODIPY FUNCTIONALIZED ANDERSON TYPE POM: SYNTHESIS, CHARACTERIZATION AND PHOTOPHYSICAL PROPERTIES..... | |
| Seda CETINDERE | 23 |
| <u>4</u> -The Biosphere Self-Organization Attractors drive perfect order homeostasis reactions to link bioenergetic with functionally activate oxygen and carbon dioxide molecules..... | |
| Aris Kaksis | 27 |
| <u>5</u> -GAS SEPARATION PROPERTIES OF MIXED MATRIX MEMBRANES PREPARED WITH GRAPHENE OXIDE | |
| Sevgi ÇANÇA, Sennur DENİZ,..... | 33 |

ANTIOXIDANT ACTIVITY of *RUMEX PATIENTIA* L. LEAVES and ANALYSIS of ITS POLYPHENOL CONTENTS by LC-MS/MS

Derya ALTINTAS¹, Yesim YESILOGLU²,

¹ Trakya University, Arda Vocational College, Edirne, Turkey,
deryaaltintas@trakya.edu.tr

² Trakya University, Faculty of Pharmacy, Edirne, Turkey,
yesimyesiloglu@trakya.edu.tr

Abstract

Rumex patientia L. is generally known under the name “labada” in Turkey. It is a plant of Polygalaceae family and its leaf is a significant source of natural antioxidant of ascorbic acid [1] [2]. Furthermore, the leaves of the *Rumex* have an analgesic, anticancer, antihypertensive, antipyretic and anti-inflammatory effects [3]. The antioxidant and phytochemical properties of *Rumex patientia* L. were examined in this study. The antioxidant and radical scavenging activities of water extract of dried leaves (WEDL), methanol extract of dried leaves (MEDL), water extract of fresh leaves (WEFL) and methanol extract of fresh leaves (MEFL) were determined using various *in vitro* methods including ferric thiocyanate (FTC) method, chelating capability on Fe⁺², ferric ions reducing capacity (FRAP) and 2,2'-azino-bis(3-ethylbenzothiazoline-6-sulfonic acid) (ABTS.+) scavenging assay. LC-MS/MS was used to analyse extracts compounds. Total phenolic and flavonoid contents were determined as mg of gallic acid equivalent per g of *Rumex patientia* L. extract. The results were evaluated in comparison with antioxidants such as α -tocopherol, butylated hydroxyanisole (BHA), ascorbic acid and butylated hydroxytoluene (BHT) and data from the similar plant samples in literature. By means of this study, it was concluded that on account of its rich rutin content, the leaves of this plant could be used *in vitro* pharmacology studies. In conclusion, this study confirms that *Rumex patientia* L. leaves could be used in medicine as a natural antioxidant instead of synthetic antioxidants.

Key Words: Antioxidant; *Rumex patientia*; LC-MS/MS; Radical scavenging; Rutin.

1. Introduction

Free radicals have one uncoupled electron in their outermost orbital and this electron can be more than one [4]. Oxygen producing radicals compose reactive oxygen species (ROS) such as superoxide and hydroxyl radical. Singlet oxygen and hydrogen peroxide are non-free radicals. As a result of the increase in ROS, oxidative stress occurs and this causes the cell damaging in biological systems. ROS can lead to many diseases such as cancer, diabetes, hypertension, cardiovascular diseases [5]. Plants and their products have rich polyphenolic compound and antioxidant potential [6] [7]. Therefore, they play a significant role in the cell [8].

There are approximately 200 species of genus *Rumex* all over the world. The leaves of the *Rumex* are used in traditional medicine [3].

In this study, radical scavenging and antioxidant properties of *Rumex patientia* L. were determined with various analytical methods. Furthermore, one other important feature of this study is the quantites of phenolic compounds such as quercetin, syringic acid, gallic acid, rutin, protocatechuic acid, abscisic acid, jasmonic acid, 2,5-dihydroxybenzoic acid, caffeic acid, salicylic acid, trans-ferulic acid and p-coumaric acid in WEDL and WEFL using LC-MS/MS.

2. Materials and Methods

2.1. Sample preparation

For water extraction, 25 g of dried and fresh *Rumex patientia* leaves were extracted with boiling water (0.5 L) for 30 minutes. These extracts were filtered through filter paper and they were frozen for later use and then were lyophilized by lyophilizator. For methanol extraction, 25 g of fresh and dried *Rumex patientia* leaves were extracted with methanol (0.5 L) by magnetic stirrer for 3 hours. These extracts were filtered through filter paper and these filtrates were collected in an erlenmayer. The methanol was evaporated in a rotary evaporator at 40 °C. Concentration range was selected as 50-250 μ g/mL.

2.2. Total phenols compound

Total phenols compound in *Rumex patientia* extracts were established by Folin-Ciocalteu method [9]. 1 mL of *Rumex patientia* extracts were placed in test tubes. The final volumes were prepared with 0.46 L of distilled water. Three minutes after adding Folin-Ciocalteu solution (1000 μ L), Na₂CO₃ solution (2%, 3 mL) was added into the test tubes. Test tubes were vortexed for 1 minute and were kept at 25 °C for 2 hours with occasional shaking. Absorbances of *Rumex patientia* extracts were measured at 765 nm.

2.3. Total flavonoid compound

Total flavonoid compounds in *Rumex patientia* extracts were determined using previous report of Yesiloglu et al. [10]. NaNO₂ solution (1 mL, 5%) was mixed with *Rumex patientia* extracts (10 mL) and 6 minutes later, 1 mL of Al₂(NO₃)₂·9H₂O (10%) solution was transferred to the reaction mixture. Afterwards, 10 mL of NaOH solution (4.3%) which were kept at 25 °C for 6 minutes was added to the test tubes. The final volume was supplemented to distilled water (25 mL). 10 minutes later, absorbance values of these mixtures were measured at 510 nm.

2.4. LC-MS/MS analysis of phenolic contents

Polyphenolic compounds in *Rumex patientia* extracts were determined by using LC-MS/MS in accordance with the methods of Bursal et al. [11]. Acetonitrile and formic acid were used as the components of the mobile phase. Also, the flow rate of mobile phase was determined as 300 µL/minute. Gradients were programmed as solvent A [formic acid (0.1%) in acetonitrile (0.1%)] and B [formic acid (0.1%) in distilled water]. Additionally, injection volume was 10 µL. Chromatographic column temperature was adjusted as 30 °C.

2.5. FRAP assay

Fe⁺³ (ferric ion) reducing activities of *Rumex patientia* extracts were determined using previous report of Ayoub et al. [12]. Various concentrations of *Rumex patientia* extracts in distilled water (1 mL) were transferred to [K₃Fe(CN)₆] solution (2.5 mL of 1% solution) and phosphate buffer solution (2.5 mL of 0.2 M solution, pH 6.6). These mixtures were incubated for 20 minutes in a water bath at 50 °C. After that, TCA solution (2.5 mL of 10% solution) was added to this reaction mixture which was centrifuged at 2000 rpm for 10 minutes. Supernatant (2.5 mL) was mixed with FeCl₃ solution (0.5 mL of 0.1% solution) and distilled water (2.5 mL). Absorbances of *Rumex patientia* extracts were recorded at 700 nm.

2.6. Fe⁺² chelating ability

Ferrous chelating activities of *Rumex patientia* extracts were determined following the method of Dastmalchi et al. [13]. 0.4 mL of *Rumex patientia* extracts were mixed with 200 µL ferrozine solution (5 mM) and 50 µL of FeCl₂ solution (2 mM). The final volumes were supplemented to ethanol (4 mL). Then, these mixtures were vortexed for 1 minute and incubated at 25 °C. 10 minutes later, absorbances of samples were measured at 562 nm.

2.7. FTC method-total antioxidant capacity

The inhibition effects of *Rumex patientia* extracts on linoleic acid peroxidation were determined using the ferric thiocyanate method of Jiang et al. [14]. Sample solution (2.5 mL) was mixed with linoleic acid emulsion (2.5 mL). These mixtures were vortexed for 1 minute and then incubated in darkness at 37 °C. Following the incubation, these mixtures (0.1 mL) were diluted with ethanol solution (3.7 mL, 75%). Then, 100 µL of ammonium thiocyanate solution (30%) was transferred into the test tubes. 3 minutes later, FeCl₂ solution (0.1 mL, 30%) was added to this mixture. After 5 minutes, absorbances of extracts and standards were measured at 500 nm. The process was repeated every 12 hours until a maximum absorbance value was recorded.

2.8. ABTS⁺ scavenging ability

ABTS⁺ scavenging effects of *Rumex patientia* extracts were determined following previous report of Abdel-Hady et al. [15]. with a minor modification. *Rumex patientia* extracts (3 mL) were combined with ABTS⁺ solution (1 mL, 7 mM). Afterwards, this solution was incubated at 25 °C for 30 minutes. Following the incubation, absorbances of samples were recorded at 734 nm.

3. Results and discussion

3.1. Total phenols and flavonoid compounds

The total phenolic content of WEFL (36.12 ± 0.65 mg GAE/g *Rumex patientia* extract) was higher than that of MEFL (26.94 ± 0.91 mg GAE/g *Rumex patientia* extract). The total flavonoid contents of MEFL and MEDL were established as 31.55 ± 0.84 and 21.05 ± 0.74 mg GAE/g *Rumex patientia* extract. In addition, flavonoid compound of WEFL (49.15 ± 0.29 mg GAE/g *Rumex patientia* extract) was higher than that of WEDL (26.65 ± 0.14 mg GAE/g *Rumex patientia* extract).

3.2. LC-MS/MS analysis of phenolic contents

Phenolic contents in WEFL and WEDL were found to be gallic acid (73.10 and 63.19 ng/g), protocatechuic acid (203.21 and 180.54 ng/g), 2,5-dihydroxybenzoic acid (81.48 and 79.34 ng/g), caffeic acid (6831.43 and 6868.89 ng/g), salicylic acid (17.21 and 17.27ng/g), syringic acid (166.20 and 143.96 ng/g), trans-ferulic acid (5403.27 and 5547.49 ng/g), rutin (11981.19 and 12087.08 ng/g), p-coumaric acid (767.92 and 812.37 ng/g), quercetin (24.21 and 21.22 ng/g), abscisic acid (601.97 and 534.39 ng/g), jasmonic acid (152.65 and 153.81 ng/g), respectively. These results revealed that the main phenolic compound, was rutin in both extracts. Rutin has pharmacological functions including anti-inflammatory, antibacterial, antiallergic, antiviral and antiprotozoal activities [3].

3.3. FRAP assay

The reducing powers of WEFL (0.075 ± 0.024), WEDL (0.063 ± 0.017), MEFL (0.097 ± 0.014) and MEDL (0.093 ± 0.012) were concentration dependent and were found to be lower than those of BHA (0.162 ± 0.033), BHT (0.143 ± 0.019), α -tocopherol (0.154 ± 0.028) and ascorbic acid (0.160 ± 0.014) at 250 $\mu\text{g/mL}$. These results revealed that MEFL and MEDL had a considerable Fe^{+3} reducing potential.

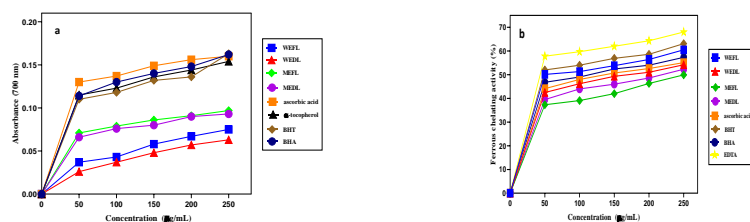


Fig. 1. (a) Fe^{+3} reducing powers of samples; (b) Ferrous chelating activities of samples

3.4. Chelating activity

All the samples had high levels of metal chelating effects. BHA, EDTA, ascorbic acid, BHT, WEFL, WEDL, MEFL and MEDL were established as 57.30 ± 0.16 , 68.00 ± 0.67 , 55.10 ± 0.44 , 63.10 ± 0.34 , 60.50 ± 0.11 , 54.00 ± 0.02 , 49.90 ± 0.19 , 52.30 ± 0.07 at 250 $\mu\text{g/mL}$. These results revealed that *Rumex patientia* extracts had a metal chelation effect but were lower than BHA and EDTA.

3.5. FTC method - total antioxidant capacity

The total antioxidant activities of standards and *Rumex patientia* extracts followed the order: MEDL (83.81%) > WEDL (83.30%) > MEFL (81.50%) > WEFL (79.31%) > α -tocopherol (74.68%) > ascorbic acid (74.30%) > BHT (73.66%) > BHA (69.29%) at 250 $\mu\text{g/mL}$. These results indicated that *Rumex patientia* extracts had a significant antioxidant activity.

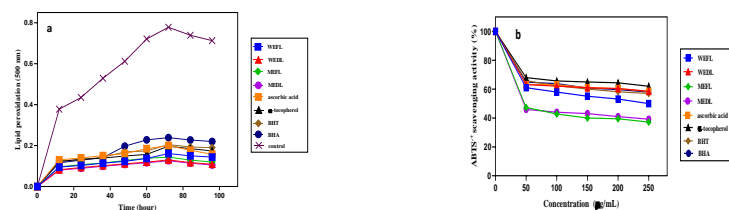


Fig. 2. (a) Lipid peroxide levels of samples at 250 $\mu\text{g/mL}$; (b) ABTS^{+} scavenging activities of samples

3.6. ABTS^{+} scavenging ability

ABTS^{+} scavenging effects of samples followed the order: α -tocopherol (68%) > BHT (65.90%) > BHA (64.90%) > ascorbic acid (63.20%) = WEDL (63.20%) > WEFL (61.00%) > MEFL (47.00%) > MEDL (46.00%) at 50 $\mu\text{g/mL}$. Although WEDL seemed to have a stronger scavenging potency, it was established that this potency was lower than that of α -tocopherol.

4. Conclusion

The antioxidant activities of fresh and dried samples of *Rumex patientia* L. leaves were determined by preparing methanol and water extracts. It was established in various *in vitro* experiments that these extracts exhibited effective antioxidant capacities. And these experimental results were compared with the results of antioxidant substances which were used as standard. Furthermore, through the analysis of LC-MS/MS, the quantities of quercetin, syringic acid, gallic acid, rutin, protocatechuic acid, abscisic acid, jasmonic acid, 2,5-dihydroxybenzoic acid, caffeic acid, salicylic acid, trans-ferulic acid and p-coumaric acid which both WEDL and WEFL contained were determined. It was established that rutin was the main phenolic compound in both extracts. By means of this study, it was concluded that on account of its rich rutin content, the leaves of this plant could be used *in vitro* pharmacology studies. In conclusion, this study confirms that *Rumex patientia* L. leaves could be used in medicine as a natural antioxidant instead of synthetic antioxidants.

5. References

- [1] Kılıc I, Yesiloglu Y, Bayrak Y, Gulen S, Bakal T. Antioxidant Activity of *Rumex conglomeratus* P. Collected from Turkey. *Asian J Chem* 2013;**25**:9683-9687.
- [2] Uzun M, Demirezer L. Anti-aging power of *Rumex crispus* L.: Matrix metalloproteinases inhibitor, sun protective and antioxidant. *South Afr J Bot* 2019;**124**:364-371.
- [3] Spinola V, Llorent-Martinez E, Castilho P. Inhibition of α -amylase, α -glucosidase and pancreatic lipase by phenolic compounds of

- Rumex maderensis (Madeira sorrel). Influence of simulated gastrointestinal digestion on hyperglycaemia-related damage linked with aldose reductase activity and protein. *LWT-Food Sci Technol* 2020;**118**:108727.
- [4] Polat L, Goren A, Namiesnik J, Gorinstein S, Gulcin I. LC-MS/MS analysis antioxidant and anticholinergic properties of galanga (*Alpinia officinarum* Hance) rhizomes. *Ind Crop Pro* 2015;**74**:712-721.
- [5] Li H B, Wong C C, Cheng K W, Chen F. Antioxidant properties in vitro and total phenolic contents in methanol extracts from medicinal plants. *LWT-Food Sci Technol* 2008;**41**:385-390.
- [6] Yesiloglu Y, Kılıç I, Sit L. In vitro antioxidant activity and total phenolic content of various extracts of *Satureja hortensis* L. collected from Turkey. *Asian J Chem* 2013;**15**:8311-8316.
- [7] Boo H O, Heo B G, Gorinstein S, Chan S U. Positive effects of temperature and growth conditions on enzymatic antioxidant status in lettuce plants. *Plant Sci* 2011;**181**:479-484.
- [8] Comert E D, Gokmen V. Antioxidants bound to an insoluble food matrix: their analysis, regeneration behavior and physiological importance. *Compr Rev Food Sci Food Saf* 2017;**16**:382-399.
- [9] Unuofin J O, Otunola G, Afolayan A. Polyphenolic content, antioxidant and antimicrobial activities of *Vernonia mespilifolia* Less. Used in folk medicine in the Eastern Cape Province, South Africa. *J Evid-Base Integr Med* 2018;**23**:1-9.
- [10] Yesiloglu Y, Sit L. Antioxidants properties of various solvent extracts from purple basil. *Spectrochim Acta A* 2012;**95**:100-106.
- [11] Bursal E, Koksal E, Gulcin I, Bilsel G, Goren A C. Antioxidant activity and polyphenol content of cherry stem (*Cerasus avium* L.) determined by LC-MS/MS. *Food Res Int* 2013;**51**:66-74.
- [12] Ayoub L, Hassan F, Hamid S, Abdelhamid Z, Souad A. Phytochemical screening antioxidant activity and inhibitory potential of *Ficus carica* and *Olea europaea* leaves. *Bioinformation* 2019;**15**:226-232.
- [13] Dastmalchi K, Dorman H D, Oinonen P P, Darwis Y, Laakso I, Hiltunen R. Chemical composition and in vitro antioxidative activity of lemon balm (*Melissa officinalis* L.) extract. *LWT-Food Sci Technol* 2008;**41**:391-400.
- [14] Jiang L, Li Y, Wang W J, Imoulan A, Yao Y J. Total phenolic content and antioxidant activity of mycelial extracts from medicinal fungus *Paecilomyces hepiali* (Ascomycetes). *Int J Med Mushrooms* 2017;**19**:35-44.
- [15] Abdel-Hady H, El-Wakil E A, Abdel-Gawad M. GC-MS analysis, antioxidant and cytotoxic activities of *Mentha spicata*. *Eur J Med Plant* 2018;**6**:1-12.

Determination of Free Energy Difference between Anomalous Solid-Liquid Phase Transitions of Silicon using Pseudo-supercritical Thermodynamic Path: A Molecular Dynamics Study

Chandan K Das*

Department of Chemical Engineering, National Institute of Technology Rourkela
Rourkela, India-769008.

*Corresponding author E-mail: dasck@nitrkl.ac.in

Abstract: Silicon shows a very different trend while melting. Melting has remained a challenging subject from a long time. Especially, predicting the melting temperature of any solid substance still exists as a problem in many cases. Recently, various studies and new rules and set of parameters have simplified things, but its mechanism is yet to be studied properly and there does not exist any generalized concept regarding this. This work is an attempt to study the mechanism of free energy difference between solid-liquid. In order to understand the free energy difference, it is important to know the interaction potential governing the silicon system. Stillinger-Weber potential is a good model for Si atoms which takes into account two and three particle interactions. Heating and quenching processes is implemented on a system of Si atoms. Free energy gap connecting phases is estimated with the help of reversible thermodynamic route. Supercritical path is constructed with the help of more than one reversible thermodynamic path. The best of my knowledge, this is first attempt to implement pseudo-supercritical reversible thermodynamic path for a system whose solid volume is higher than liquid volume at phase transition point.

Keywords: Molecular Dynamics, LAMMPS, Hysteresis Loop, Pseudo-super-critical Path, Thermodynamic Integration

1. Introduction

Phase transition is reported for many pure materials including silica and silicon. Transition point is obtained either pressure swinging or temperature swinging method. Transition temperature can also be evaluated using specific heat capacity information. Another robust technique for determination of transition point is calculation of entropy. Conventional methods like density hysteresis plot, Lindemann parameter, non-Gaussian parameter, radial distribution function, structure factor, orientation order parameter etc are employed to predict the transition point of a material.

Most of the above-mentioned methods are not accurate to predict the melting transition[1]. Estimated melting temperature is often higher compare to true melting temperature. Melting transition can be predicted more precisely using the knowledge of free energy. Transition temperature of Lennard-Jones(LJ) and sodium Chloride(NaCl) is reported from free energy information[2]. Free energy is evaluated employing thermodynamic integration. The thermodynamic route connecting solid-liquid is constructed employing reversible thermodynamic route[1,2]. Phase transformation from solid to liquid under slit[3,4] and cylindrical confinement is studied using free energy analyses[5].

In this work, I evaluate free energy gap connecting solid-liquid transitions. The best of my knowledge, this is first attempt to implement pseudo-supercritical reversible thermodynamic path for a system whose solid volume is higher than liquid volume at phase transition point. Moreover, due to very small density difference between two phases make the simulations more complicated. I present briefly the technique. (a) The liquid state is transformed into a poorly interacting liquid with the help of slowly decreasing the interatomic attractions. (b) Gaussian wells are located to the corresponding particles; simultaneously the volume is enlarged to obtain a poorly interacting oriented state. (c) Gaussian wells are removed gradually and simultaneously interatomic attractions are slowly brought back to its whole strength to obtain a crystalline state.

2. Methodology

In this work, I evaluate the free energy connecting solid-liquid state transition. The inclusive technique is described elsewhere[1]. The estimation of phase transition point from free energy analysis is combination of four stages. First step is evaluation of an approximate transition point from quenching and heating method. Free energy computation is performed with the help of pseudo-supercritical transformation path. Each step is exclusively elaborated below. Interaction potential of silicon[6] is as follows:

$$E = U_{inter}(r^N) = \sum_i \sum_{j>i} \varphi_2(r_{ij}) + \sum_i \sum_{j \neq i} \sum_{k>j} \varphi_3(r_{ij}, r_{ik}, \theta_{ijk}) \quad (1)$$

$$\varphi_2(r_{ij}) = A_{ij} \epsilon_{ij} \left[B_{ij} \left(\frac{\sigma_{ij}}{r_{ij}} \right)^{p_{ij}} - \left(\frac{\sigma_{ij}}{r_{ij}} \right)^{q_{ij}} \right] \exp \left(\frac{\sigma_{ij}}{r_{ij} - a_{ij} \sigma_{ij}} \right) \quad (2)$$

$$\varphi_3(r_{ij}, r_{ik}, \theta_{ijk}) = \lambda_{ijk} \epsilon_{ijk} [\cos \theta_{ijk} - \cos \theta_{0ijk}]^2 \exp \left(\frac{\gamma_{ij} \sigma_{ij}}{r_{ij} - a_{ij} \sigma_{ij}} \right) \exp \left(\frac{\gamma_{ik} \sigma_{ik}}{r_{ik} - a_{ik} \sigma_{ik}} \right) \quad (3)$$

The φ_2 represents two particles interaction term. The φ_3 presents three particles attraction expression. The summation in the expression are overall neighbors J and K of atom I within a truncated length a [7]. The A, B, p, and q parameters employed for two-particles attractions. The λ and $\cos \theta_0$ parameters are used only for three-

particles attractions. The ϵ , σ and a parameters employed for both cases. γ is employed for three-particles attraction. However, this is classified for pairs of atoms. The others extra parameters are dimensionless[7].

Table 1: Values of parameters used in SW potential(in metals unit)

| A | | B | | ϵ | | σ | |
|-------|-------|------|-----|------------|-------|----------|--|
| | | | | (eV) | | (Å) | |
| 7.04 | | 0.60 | | 2 | | 2 | |
| 95562 | 22245 | .80 | 1.0 | .20 | .1672 | .0951 | |

2.1 Estimation of an estimated transition temperature

To detect an approximate transition temperature, gradually heating and quenching simulations are performed for solid and liquid states, respectively[5], by employing *NPT* simulation at $P = 1.0$ bar. Afterwards, the estimated transition temperature is chosen within the metastable region at where a sudden change in the density is noticed[5].

2.2 Computation of solid-liquid free energy gap at an estimated transition point

The Helmholtz free energy gap connecting the solid and liquid states at an estimated transition point is estimated by forming a reversible way connecting the solid and liquid states with the help others reversible stages[5]. The free energy throughout the connecting route is evaluated using a known integration scheme:

$$\Delta A^{ex} = \int \langle \frac{dU}{d\lambda} \rangle_{NVT\lambda} d\lambda \quad (4)$$

while ΔA^{ex} is the gap in Helmholtz free energy. Kirkwood's coupling parameter is used by the symbol λ . Generally, λ changes in between 0 to 1. The value of $\lambda = 0$ system act as an ideal state[18]. The angled bracket is indication of ensemble average for a specific λ parameter[18]. The three stages pseudo-supercritical conversion method is represented in Fig. 1.

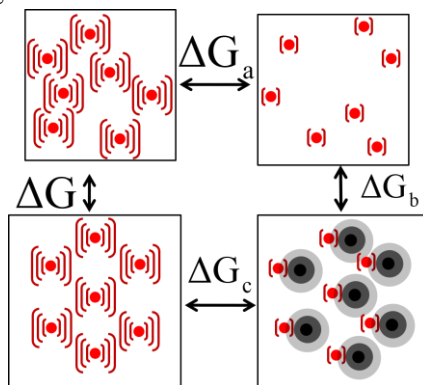


Figure : 1 presents the three stages pseudo-supercritical conversion route. (a) The liquid state is transformed into a poorly interacting liquid by slowly increasing the coupling parameter[18]. (b) Gaussian wells are located to the corresponding particles; simultaneously the volume is enlarged to obtain a poorly interacting oriented state. (c) Gaussian wells are removed gradually while coupling parameter is slowly increasing to bring back its full strength to obtain a crystalline state.

1.Stage-a

Initially, strongly attracted liquid state is transformed into a poorly interacting liquid using a coupling parameter λ , which controls interatomic potential[18] in the mentioned way:

$$U_a(\lambda) = [1 - \lambda(1 - \eta)]U_{inter}(r^N) \quad (5)$$

where $U_{inter}(r^N)$ is the interatomic interaction energy due to location of all N particles[2]. The η is a scaling parameter. The value varies $0 < \eta < 1$. The first derivative of intermolecular interaction relation produces:

$$\frac{\partial U_a}{\partial \lambda} = -(1 - \eta)U_{inter}(r^N) \quad (6)$$

2.Stage-b

During second stage, volume of liquid state is enlarged to the volume of solid state unlike other conventional substances. Enlarge volume is clearly visible in Fig. 1. Hence, length of the simulation box (L_x, L_y

and L_z) for a particular system dimension must be predetermined at the estimated transition point, either from the MHR results or hysteresis diagram. Liquid box dimension is $21.28163 \text{ \AA} (H_l)$ and solid phase dimension is $21.81412 \text{ \AA} (H_s)$. The change in simulations' box dimension confirms that pressures remain unaltered at the start of thermodynamic path and at the completion of stage-c, which is presented in Fig. 7. The interatomic interaction on the basis of λ in this stage is represented following way:

$$U_b(\lambda) = \eta U_{inter}[r^N(\lambda)] + \lambda U_{Gauss}[r^N(\lambda), r_{well}^N(\lambda)] \quad (7)$$

where $r^N(\lambda)$ and $r_{well}^N(\lambda)$ are the representation of the positions of atoms and Gaussian wells respectively[18]. U_{Gauss} presents interatomic potential because of the attraction in between the wells and corresponding particles(Eq.9). The values of parameters 'a' and 'b' are taken from Gochola's works[1]. $H(\lambda)$ denotes box dimension at any value of coupling parameter λ . Equation 8 represents change in box dimension for coupling parameter values.

$$H(\lambda) = (1 - \lambda)H_l + \lambda H_s \quad (8)$$

$$U_{Gauss}[r^N(\lambda), r_{well}^N(\lambda)] = \sum_{i=1}^N \sum_{k=1}^{N_{wells}} a_{ik} \exp[-b_{ik} r_{ik}^2(\lambda)] \quad (9)$$

$$-\frac{\partial U_{inter}}{\partial H_{xz}} = \sum_y P_{xy}^{ex} V H_{zy}^{-1} H(\lambda) = (1 - \lambda)H_l + \lambda H_s \quad (10)$$

Derived form of potential expression with respect to λ is

$$\frac{\partial U_b}{\partial \lambda} = -\sum_{x,y,z} V(\lambda) H_{zy}^{-1}(\lambda) \Delta H_{xz} (\eta P_{xy}^{ex} + \lambda P_{Gauss,xy}^{ex}) + U_{Gauss}[r^N(\lambda), r_{well}^N(\lambda)] \quad (11)$$

3. Stage-c

Stage-c is ultimate step of the pseudo-supercritical conversion method[2]. In this stage fully interacting solid configurationally phase is obtained. The interaction potential is presented of this final step in term of λ

$$U_c(\lambda) = [\eta + (1 - \eta)\lambda] U_{inter}(r^N) + (1 - \lambda) U_{Gauss}[r^N(\lambda), r_{well}^N(\lambda)] \quad (12)$$

And the derivative term can be rewritten:

$$\frac{\partial U_c}{\partial \lambda} = (1 - \eta) U_{inter}(r^N) + U_{Gauss}[r^N(\lambda), r_{well}^N(\lambda)] \quad (13)$$

3. Simulation Details

3.1 Atomic Potential Used

Stillinger-Weber Potential is a good model for Si. It considers both two-particle and three-particle interactions. The values of following parameters in metal units have been used. The potential of the silicon is provided in Eq. 1, 2 and 3. Parameters values are listed in Table. 1.

3.2 Simulation Details and Potential Model

The NPT MD simulations are conducted with the help of LAMMPS[7]. Integration time step (Δt) is 5fs for all type of simulations. The temperature is monitored using a Nose'-Hoover thermostat. The pressure is monitored using Nose'-Hoover barostat. The time relaxation is of 100ps. The pressure relaxation is of 500ps. Number of particles are simulated around 512. Cooling process is carried out gradually after each 5000,000 MD time steps. Change of temperature T is 25K for each NPT simulation. Temperature is dropped from 3000K to 500K with a decrement of 25K. Heating is also conducted same way as the quenching. Temperature range of heating is from 500K to 3000K. The Gibbs energy gap for connecting states is estimated at transition temperature using pseudo-super-critical path. For the reversible path evaluation (for the three steps of pseudo-supercritical path)as shown in figure 1, simulations are carried with *NVT* ensemble. The value of Gaussian parameters are selected in accordance with Grochola[1].

Simulations of Stage-a of the reversible thermodynamic path are initialized from a random initial co-ordinates of the particles. Total run time for each coupling parameter value is 20 ns[4]. During the stage-b of three stages, final co-ordinates of step-1 are the starting point. But, to achieve the Gaussian potential wells another 512 atoms are situated on its corresponding lattice point[2,8].

4. Results and Discussions

In this portion I try to describe output results of various parameters like density, potential energy and free energy with the change in temperature and coupling parameter(λ).

4.1 Density

In this part we describe the nature of density of the Si system as we perform heating and quenching. Quenching and heating path are not reversible, for this reason hysteresis loop is formed. That indicates first order phase transition. Density of silicon for different temperature is shown in figure 2. The plot clearly forms a hysteresis. This is an indication of first order phase change. Density plot shows anomaly behavior towards the phase transition. Metastable region is observed in middle portion of the hysteresis curve. True melting temperature lies in this loop.

4.2 Free energy

Helmholtz free energy difference between liquid and solid phase is determined using pseudo-supercritical path by constructing reversible thermodynamic paths[1]. Thermodynamics integration is performed using Gauss-quadrature integration scheme. At the beginning of the reversible path the interaction potential is changing according to Eq. 5. Integration is carried out using 10, 15 and 20 points. No significance difference is observed due to different data points. Derivative of interaction potential energy with respect to λ presents in Fig. 6 below. For the λ values they coincide as shown in figure 6. Figure 8 and 9 represent for stage-b and stage-c respectively. Figures for all the stages are smooth and reversible, so we can easily integrate it. The free energy difference connecting solid-liquid is around $-59024.2454 \pm 10 \text{ eV}$. Results are reported in Table 4 below.

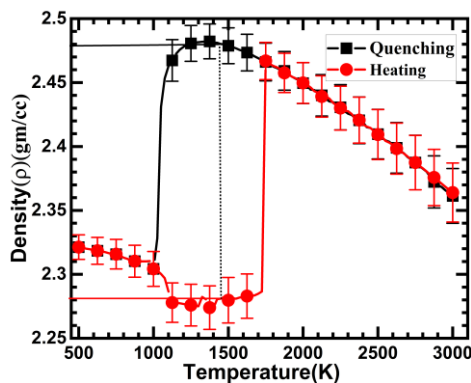


Figure 2: figure represents density vs. temperature plot. I skipped some intermediate points for better clarity. Filled square black in color presents for quenching the system whereas filled circle for heating the system. Quenching and heating curves do not follow the same path which indicates first order transition. Vertical dotted line indicates an estimated estimate transition point (T_{em}) (1450°K). Horizontal black line and red line indicate corresponding liquid density (2.477) and solid density (2.850) respectively to determine liquid phase and solid phase box dimension.

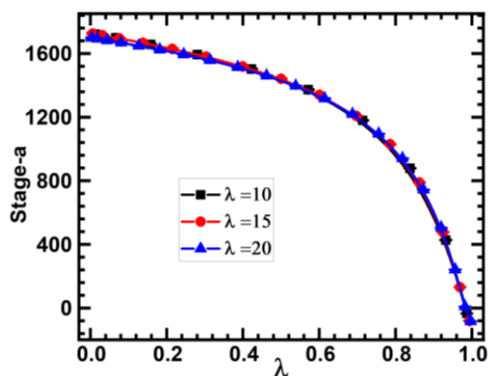


Figure: 6 $(\partial U / \partial \lambda)_{NVT\lambda}$ as a variable of λ for three λ types values (10, 15 and 20) of Stage-a for pseudo supercritical path. Thermodynamic path is smooth and reversible, hence integrable. Error is so small it submerges with symbol. There is no significant difference among them for stage-a of pseudo-supercritical transformation path

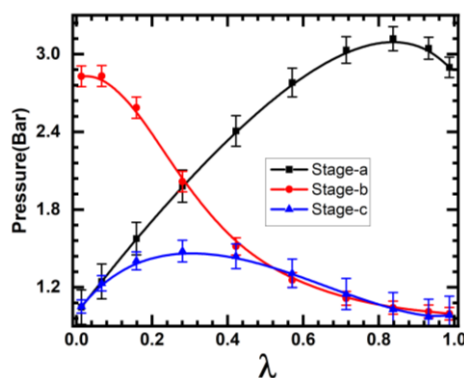


Figure : 7 Pressure at the start of stage-a and at the end of stage-c is constant. This is essential and the sufficient criteria for construction of the thermodynamic reversible paths..

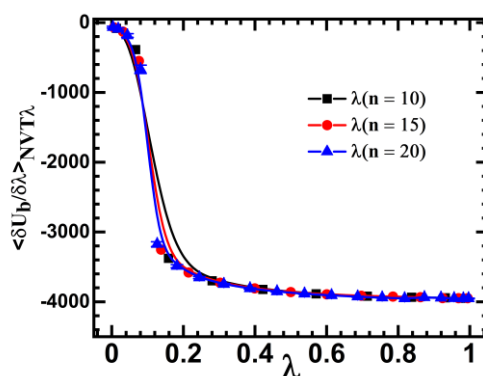


Figure : 8 $\langle \delta U / \delta \lambda \rangle_{NVT\lambda}$ as a variable of λ for ten λ of Stage-b values. Thermodynamic path is smooth and reversible, hence integrable. Error is so small it submerges with symbol.

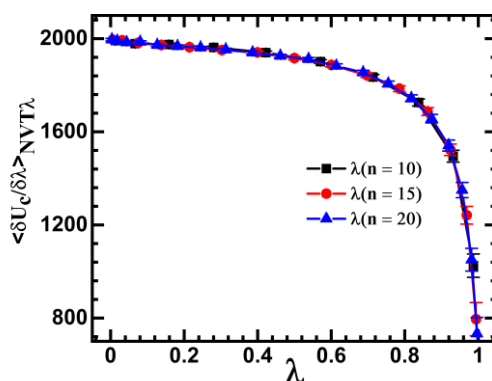


Figure : 9 $\langle \delta U / \delta \lambda \rangle_{NVT\lambda}$ as a variable of λ for three λ values for stage-c. Thermodynamic path is smooth and reversible, hence integrable.

Table: 4. Separation of the subscriptions to the gap in Gibbs free energy connecting the two states $T= 1450^\circ\text{K}$. The pressure is maintained at $P= 1$ bar for the silicon(Stillinger-Weber Potential).

| Free Energy Terms(eV) | |
|-------------------------|---------------|
| $A_s^{*ex} - A_l^{*ex}$ | 307±10 |
| $A_s^{*id} - A_l^{*id}$ | -60073 |
| $P^s \Delta V^*$ | 741.7546 |
| $G_s^* - G_l^*$ | - |
| | 59024.2454±10 |

5. Conclusion

Various methods have been employed and we have been successful in observing the phase transition of silicon, depending on various parameters.

Also, keeping in mind the traditional meaning of solid to liquid phase transition, the jump in potential energy is also used to indicate the melting stage of any substance. This jump is seen at 1700-1800 K for decreasing temperature and 2400-2500 K for increasing temperature. Anomaly behavior is observed in density for silicon system, which make more complicated to implement pseudo-supercritical thermodynamic path.

Estimation of the Gibbs free energy is performed with the help of pseudo-supercritical reversible thermodynamic cycle. The construction of supercritical path is combination of three stages. For each step of thermodynamics integration is applied using 10, 15 and 20 points. The thermodynamics integration is insignificance with respect to number of data points. Accuracy of determined melting temperature from free energy analysis is better comparing any other methods. This is a very clear indication of how the break-down of lattice occurs on heating a substance.

Acknowledgements:

This work is supported by National Institute of Technology Rourkela, Government of India

6. References

1. Grochola, G., *Constrained fluid λ -integration: Constructing a reversible thermodynamic path between the solid and liquid state*. J. Chem. Phys., 2004. **120**: p. 2122.
2. Eike, D.M., J.F. Brennecke, and E.J. Maginn, *Toward a robust and general molecular simulation method for computing solid-liquid coexistence*. J. Chem. Phys., 2005. **122**: p. 014115.
3. Das, C.K. and J.K. Singh, *Effect of confinement on the solid-liquid coexistence of Lennard-Jones Fluid*. J.

- Chem. Phys., 2013. **139**(17): p. 174706.
4. Das, C.K. and J.K. Singh, *Oscillatory Melting Temperature of Stockmayer Fluid in Slit Pores*. J. Phys. Chem. C., 2014. **118**(36): p. 20848–20857.
 5. Das, C.K. and J.K. Singh, *Melting transition of Lennard-Jones fluid in cylindrical pores*. J. Chem. Phys., 2014. **140**(20): p. 204703-1 - 204703-9.
 6. Stillinger, F.H. and T.A. Weber, *Computer simulation of local order in condensed phases of silicon*. Phys. Rev. B, 1985. **31**(8): p. 5262-5271.
 7. J, P.S., *Fast Parallel Algorithms for Short-Range Molecular Dynamics*. J. Comp. Phys., 1995. **117**: p. 1-9.
 8. Das, C.K. and J.K. Singh, *Melting transition of confined Lennard-Jones solids in slit pores*. Theor Chem Acc, 2013. **132**: p. 1351.

PHENOL CONTAINING BODIPY FUNCTIONALIZED ANDERSON TYPE POM: SYNTHESIS, CHARACTERIZATION AND PHOTOPHYSICAL PROPERTIES

Seda CETINDERE¹

¹Gebze Technical University Department of Chemistry Gebze, Kocaeli, TURKEY
sdemirer@gtu.edu.tr

Abstract

Anderson type POMs are among the most known oxo compounds. Functionalization of POMs with organic groups such as BODIPY, provides a strategy to achieve POM-based hybrid materials. They combine the advantages of organic molecules such as good solubility and easy functionalization together with chemical stability and high redox activity of inorganic POM clusters. This study aims to functionalization of Anderson type POM with phenol containing BODIPY dye and investigation of its photophysical properties to see its usability as a photosensitizer in solar energy conversion processes.

Key Words: BODIPY; POM, Anderson, phenol, photophysical properties.

1. Introduction

Polyoxometalates (POMs) are inorganic metal-oxo cluster anions of the general formula $[M_xO_y]^{n-}$ consisting of two or more high-valent transition metals (M) such as W, V, Mo, Nb, Ta, which are linked via bridging μ -oxo-ligands. The early transition metals are incorporated into the cluster as oxoanions in a high oxidation state (d^0 , d^1) and are called addenda atoms. Together with terminal oxo-ligands and the sharing μ -oxo-ligands they form coordination polyhedra of the type $[MO_y]$ ($y = 4-7$). The formation of POMs follows a unique self-assembly process of these preformed building blocks which can be linked by sharing corners, edges and more rarely faces. The first POM reported was a phosphomolybdate, namely $[PMo_{12}O_{40}]^{3-}$, which was obtained by Berzelius in 1826 from ammonium molybdate $(NH_4)_2MoO_4$ with an excess of phosphoric acid [1]. Today an unrivalled structural diversity of POM clusters like Anderson, Keggin, Dawson, Lindqvist etc. is known (Fig. 1).

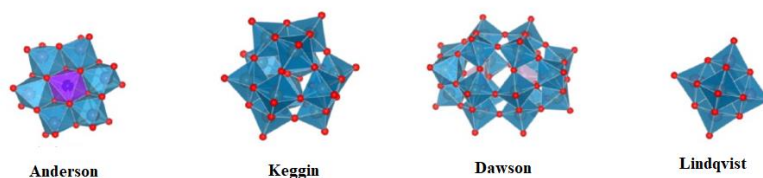


Fig. 1. Different structure types of POMs

The structural versatility of POMs is the reason for their rich chemistry and the ability to form systems ranging in size from the nano- to the micrometer scale [2]. They exhibit an almost unmatched range of physical and chemical properties, e.g., superacidity [3], photo or electrochromism [4], magnetism [5] and ionic conductivity [6-7]. For this reason, POMs have attracted growing interest among the scientific worlds. During the last few decades, they also became relevant to analytical chemistry, [8] catalysis and medicine [9-11] and are of great interest to materials science as novel materials.

Reactions of POMs with organic moieties like boron dipyrromethene (BODIPY) dyes provides a smart strategy to achieve POM-based inorganic-organic hybrid materials. They combine advantages of organic molecules such as good processability and fine-adjustable structures together with chemical stability and high redox activity of inorganic POM clusters [12]. BODIPYs are fluorescent organic dyes which have interesting spectral properties such as high quantum yields (0.6-1.0), large extinction coefficients ($60000-80000 M^{-1}cm^{-1}$) and narrow emission bands. On the other hand, absorption and emission properties of these dyes can be adjustable by substitution of different groups into the BODIPY core [13].

In this study, the novel compound (BPOM) synthesized by the reaction of Anderson type POM (POM_{Cl}) and phenol containing BODIPY (PCB) (Fig. 2) and then characterized by using FT-IR, MALDI-MS, 1H NMR

spectroscopy techniques and elemental analysis. Photophysical properties of BPOM were investigated by UV-visible and fluorescence spectroscopy.

2. Experimental

POM_{Cl} [14] and PCB [15] were synthesized according to the literature procedures.

2.1. Synthesis of BPOM

Argon gas was applied to the 100 mL reaction flask and dry MeCN (50 mL) was put and bubbled in the flask. POM_{Cl} (80 mg, 0.039 mmol, 1 equiv.) was put in the reaction flask and dissolved in DMF. PCB (40 mg, 0.12 mmol, 4 equiv.) was added into the reaction flask. The reaction mixture was stirred under reflux for 48h. The reaction mixture was controlled with IR (Fig. 3) and when the -OH peak was disappeared, the reaction was finished. The mixture was precipitated in diethyl ether. Collected products in diethyl ether were centrifuged and then brownish, orange-colored solid fractions were collected and dried in air. BPOM (77 mg, 0.029 mmol) was obtained with 64% yield. Elemental analysis in wt.-% for (C₁₆H₃₆N)₃(MnMo₆O₁₈((OCH₂)₃C₂₂H₂₁N₃O₂F₂B)₂) (calcd.): C 44.34 (44.54), H 6.58 (6.18), N 4.85 (4.77). MALDI MS (m/z) for C₉₈H₁₆₂B₂F₄MnMo₆N₉O₂₈: 2642.43 (Calc.), 2643.60 ([M+H]⁺ Found) (Fig. 4). ¹H NMR (500 MHz, MeCN-d₃): δ (ppm) = 65.94 (s, br, 12H, -OCH₂ in POM cluster), 7.96 (d, 4H, H_{aro}), 7.19 (d, 4H, H_{aro}), 6.09 (s, 4H, H_{pyr}), 5.37 (br, 2H, -NH-), 5.20 (d, 4H, -O-CH₂-), 3.09 (br, 24H, -CH₂- (TBA)), 2.69 (br, 4H, -CH₂-), 2.47 (s, 6H, CH₃), 2.23 (s, 18H, -CH₃), 1.59 (br, 24H, -CH₂- (TBA)), 1.43 (br, 24H, -CH₂- (TBA)), 0.96 (br, 36H, -CH₃ (TBA)) (Fig. 5).

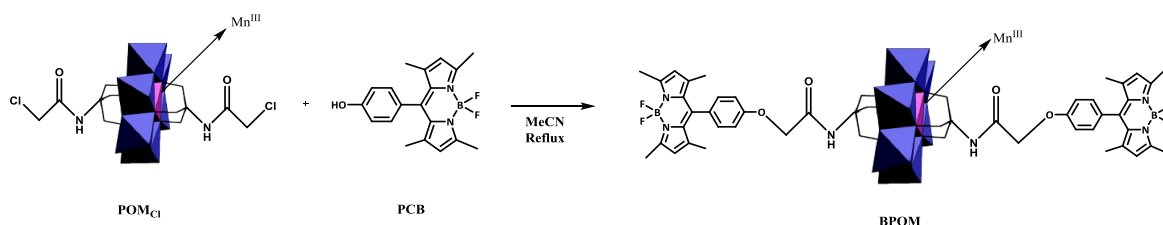


Fig. 2. Synthetic pathway of BPOM

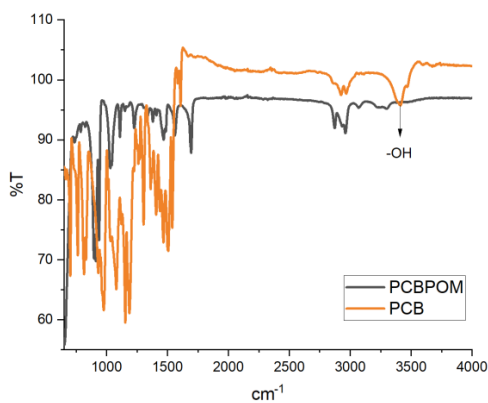


Fig. 3. FT-IR spectra of compounds PCB and BPOM

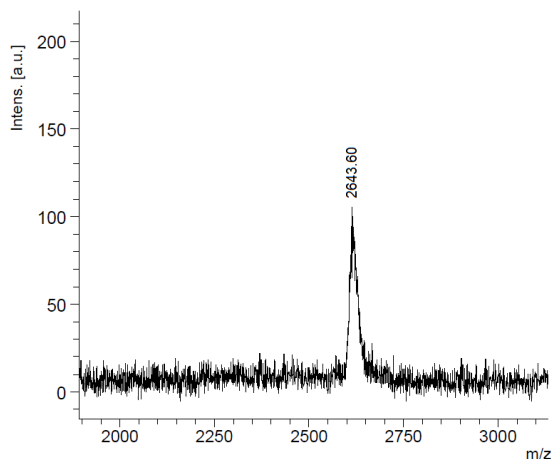


Fig. 4. MALDI MS spectra of BPOM

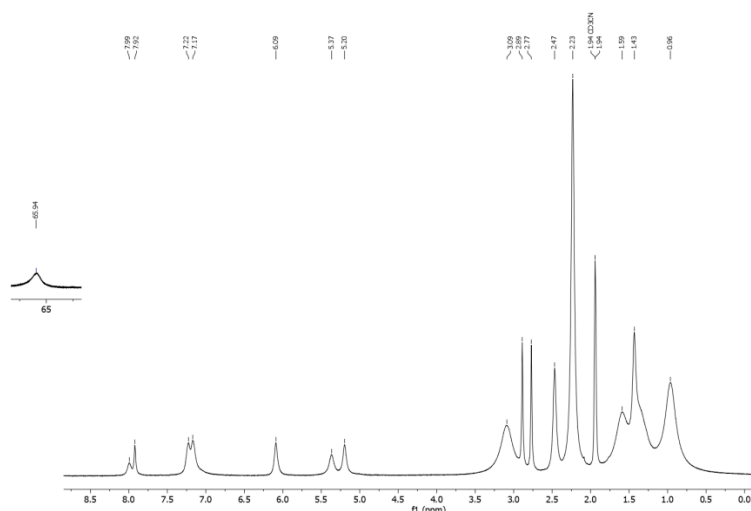


Fig. 5. ¹H NMR spectra of BPOM

2.2. Photophysical properties of BPOM

Photophysical properties of BPOM were investigated by using UV-visible absorption and fluorescence spectroscopy techniques (Fig. 6). The absorption and fluorescence properties of BPOM have been studied in MeCN, because BPOM has good solubility in MeCN rather than other organic solvents. According to the Fig. 6a, the absorption maxima of BPOM was observed at 501 nm like its precursor BODIPY. According to the Fig. 6b, the emission maxima of BPOM was observed at 506 nm which is attributed to the BODIPY moieties, because free POM_{C1} do not give any fluorescence signal.

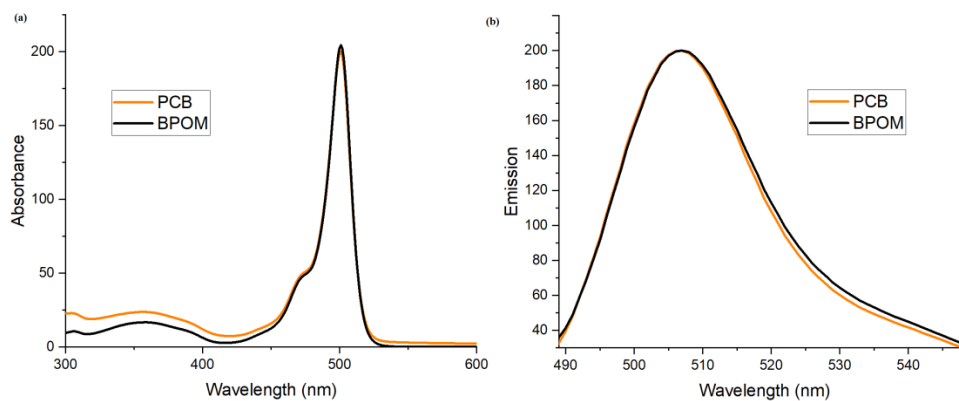


Fig. 6. (a) Normalized absorption; (b) normalized emission spectra of compounds PCB and BPOM. (Excitation wavelength: 475nm).

3. Results and Future Work

A novel compound (BPOM) was synthesized by functionalization of Anderson type POM with phenol containing BODIPY dye and fully characterized. Photophysical properties of this novel compound were investigated by using UV-visible absorption and fluorescence spectroscopies. According to these investigations, BPOM dyad retains the unique photophysical properties of BODIPY showing its promise as a photosensitizer in solar energy conversion processes. Future studies will include investigation of electrochemical properties of BPOM to see its redox properties and photocatalytic experiments will be done to see its performance as a photosensitizer in solar energy conversion.

References

- [1] J. Berzelius, *Ann. Phys. Chem.* 1826, 82, 369.
- [2] M. Ammam, *J. Mater. Chem.* 2013, Advance Article.

- [3] J. Arichi, M. Eternot, B. Louis, *Catalysis Today*, 2008, 138, 117-122.
- [4] B. Xu, L. Xu, G. Gao, W. Guo, S. Liu, J. *Colloid Interface Sci.*, 2009, 330, 408-414.
- [5] J. M. Clemente-Juan, E. Coronado, A. Gaita-Arino, *Chem. Soc. Rev.*, 2012, 41, 7464-7478.
- [6] H. Gao, K. Lian, J. *Electrochem. Soc.*, 2011, 158, A1371-A1378.
- [7] H. Gao, H. Wu, K. Lian, *Electrochem. Commun.*, 2012, 17, 48-51.
- [8] M. T. Pope, A. Muller, *Angew. Chem. Int. Ed.*, 1991, 30, 34-48.
- [9] T. Yamase, *J. Mater. Chem.*, 2005, 15, 4773-4782.
- [10] B. Hasenknopf, *Front.Biosci.*, 2005, 10, 275.
- [11] M. Aureliano, *Dalton Trans.*, 2009, 9093-9100.
- [12] Pope MT, Jeannin Y, Fournier M (1983), Heteropoly and isopoly oxometalates, Springer-Verlag Berlin, Heidelberg.
- [13] Loudet A, Burgess K, *Chemical Reviews*, 2007, 107:4891-4932.
- [14] S. Vanhaecht, J. Jacobs, L. V. Meervelt, T. N. Parac-Vogt. *Dalton Trans.*, 2015, 44, 19059–19062.
- [15] C. Zhang, J. Zhao, S. Wu, Z. Wang, W. Wu, J. Ma, S. Guo, L. Huang, *J. Am. Chem. Soc.*, 2013, 135, 10566–10578.

The Biosphere Self-Organization Attractors drive perfect order homeostasis reactions to link bioenergetic with functionally activate oxygen and carbon dioxide molecules.

Aris Kaksis,

dep. Human Physiology and Biochemistry, Riga Stradin's University and e-mail: aris.kaksis@rsu.lv,

Abstract.

The quantitative studies for oxygen and carbon dioxide functional activity reveal multiply generated Self-Organization Attractors which create and maintain order the homeostasis: water concentration $[\text{H}_2\text{O}]=55.3 \text{ mol/Liter}$, $\text{pH}=7.36$, enzyme Carbonic Anhydrase reactivity, air oxygen level 20.95 % O_2 [1], osmolar concentration 0.305 M, ionic strength 0.25 M, temperature 310.15 K degree etc. that make oxygen fire safe and $\text{CO}_{2\text{aqua}}$ functional active for Life Biochemistry.

Air oxygen level 20.95 % O_2 [1] dissolute in organism forming arterial concentration $[\text{O}_{2\text{aqua}}]$ safe for Bioenergetic as Self-Organization Attractor [3] sustaining isooxia.

Thermodynamic indicate Biosphere indispensability to reach Self-Organization Attractor values. Destiny is trend to minimum of free energy change in homeostasis. Attractors made functionally active molecules Self-Organize the perfect reactions order in homeostasis. [2,3,4] Deviation from Attractor values disorder the homeostasis. Chaos stop the homeostasis which disappears as extinct from Biosphere.

Key Words: Biosphere, Thermodynamics, Self-Organization, Attractors, Bioenergetics.

1. Introduction.

Ilya Prigogine in 1954 demonstrate the isolate mixture of compounds in reactions trend reach Free energy change minimum at equilibrium state. [2] Prigogine in 1977 declares: equilibrium state is Attractor for non-equilibrium state in reactions mixture of compounds. [3,4] Prigogine explains perfect order formation as Self-Organization Attractors for Universe and Sciences.

About Universe creation in perfect order Maria Kuman: „The nonlinear no equilibrium theory of Prigogine is also called The Chaos Theory because it claims that our Universe was created in perfect order out of the chaos.”. [5] Chaos is just apparent disorder. The Biosphere belongs to our human civilization and is the part of perfect Universe.

Attractors create perfect order with functionally active molecules. Self-Organization with Attractors in dissipative structures makes the homeostasis order. Biochemistry Thermodynamic studies indicate Attractor vales of two types: the primary Attractor values are common for Life Biosphere (air oxygen level 20.95 % O_2 , Carbonic Anhydrase CA reactivity), the secondary Attractor values are for individual organisms (generate concentration gradients, isooxia - homeostasis Norma) and multipurpose Attractor values ($\text{pH}=7.36$, water and its concentration).

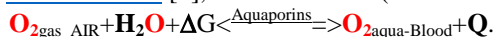
Generally, water is common multipurpose Attractor for Life Biosphere. Non-equilibrium homeostasis work in water medium and water is as substrate, is as product and is common for homeostasis medium so for environment.

1.1.1. Four Attractors and decreased Oxygen power for functional activity isooxia.

Water triplet state of oxygen, its concentration $[\text{H}_2\text{O}]=55.3 \text{ mol/Liter}$, air oxygen level 20.95 % for five hundred million Years, $\text{pH}=7.36$ for the concentration $[\text{H}_3\text{O}^+]=10^{-7.36} \text{ M}$.

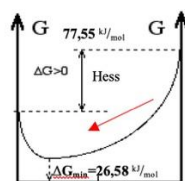
Water solution oxygen keeps **triplet** state. Oxygen no reaction with water, prevent singlet formation.

Air oxygen 20.95 % concentration as Attractor forms functional active solutions arterial $[\text{O}_{2\text{aqua}}]=6 \cdot 10^{-5} \text{ M}$ and venous $[\text{O}_{2\text{aqua}}]=0.426 \cdot 10^{-5} \text{ M}$ concentrations [6], what is isooxia (homeostasis Norma).



Rotating Electrode Method detect oxygen solubility: [7]

$$K_{\text{sp}} = \frac{[\text{O}_{2\text{aqua}}]}{[\text{O}_{2\text{gas}}] \cdot [\text{H}_2\text{O}]} = K_{\text{O}_2} / [\text{H}_2\text{O}] = 1.22 \cdot 10^{-3} / 55.3 = 2.205 \cdot 10^{-5} \text{ and}$$



Reactant $\text{O}_{2\text{gas}} + \text{H}_2\text{O}$ A+B 50 % C products $\text{O}_{2\text{aqua-Blood}}$.

Figure 1. Exothermic and endoergic Hess oxygen solubility having Free energy change positive $\Delta G_{\text{Hess}}=77.55 \text{ kJ/mol}$, but minimized Free energy change $\Delta G_{\text{min}}=\Delta G_{\text{eq}}=-26.58 \text{ kJ/mol}$ reaching solubility product equilibrium mixture: $K_{\text{sp}}=2.205 \cdot 10^{-5}$.

Free energy change minimum in expression is:

$$\Delta G_{sp} = -R \cdot T \cdot \ln(K_{sp}) = -8.3144 \cdot 298.15 \cdot \ln(2.205 \cdot 10^{-5}) = 26.58 \text{ kJ/mol.}$$

Water solution oxygen free energy content 26.58 kJ/mol increases.

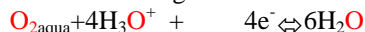
Table 1. Standard ΔH°_{Hess} , ΔS°_{Hess} and ΔG°_{Hess} values of formation from elements, at ionic strength 0.25 M, at 298.15 K degree. [1] **Biochemistry thermodynamic 2006** [8] in bold are data for pH=7.36.

| Substance | ΔH°_{Hess} , kJ/mol | ΔS°_{Hess} , J/mol/K | ΔG°_{Hess} , kJ/mol |
|------------------------------------|------------------------------------|-------------------------------------|------------------------------------|
| O₂aq | -11.70 | -94.2 | 16.40 |
| O ₂ aq | -11.715 | 110.876 | 16.4 |
| O ₂ gas | 0 | 205.152 | -61.166 |
| H ₃ O ⁺ | -285.81 | -3.854 | -213.275 |
| OH ⁻ | -230,015 | -10,9 | -157,2 |
| H ₂ O | -285.85 | 69.9565 | -237.191 |
| H₂O | -286.65 | -453.188 | -151.549 |
| CO ₂ aq | -413,798 | 117,5704 | -385,98 |
| CO ₂ gas | -393,509 | 213,74 | -394,359 |
| HCO₃⁻ | -692,495 | -494,768 | -544,969 |
| HCO ₃ ⁻ | -689,93 | 98,324 | -586,94 |

Hess law calculations for: Enthalpy **exothermic**: $\Delta H_{Hess} = \Delta H^{\circ}_{O_{2aq}} - \Delta H^{\circ}_{O_{2gas-AIR}} = -11.7 \text{ kJ/mol}$; for Entropy $\Delta S_{Hess} = \Delta S^{\circ}_{O_{2aq}} - \Delta S^{\circ}_{O_{2gas-AIR}} = -299 \text{ J/mol/K}$; and for Free energy ;

$$\Delta G_{Hess} = \Delta H_{Hess} - T \cdot \Delta S_{Hess} = -11.7 - 298.15 \cdot (-0.299352) = 77.55 \text{ kJ/mol endoergic.}$$

Blood plasma oxygen is strong oxidant according half reaction standard potential $E_o = 1.383 \text{ Volts}$ [2]



oxidized form free electrons reduced form.

1) Three **Attractors**: air oxygen O₂ 20.95% , water concentration [H₂O] = $10^{996.23}/18 = 55.3 \text{ M}$ and pH=7.36 minimize Free energy content in one mol of O₂aq, as arterial blood concentration [O₂aq] = $6 \cdot 10^{-5} \text{ M}$ and pH=7.36 for the concentration [H₃O⁺] = $10^{-7.36} \text{ M}$.

$$E_{O_2} = E^{\circ}_{O_2} + 0.0591/4 \cdot \lg([O_{2aq}] \cdot [H_3O^+]^4 / [H_2O]^6) = 1.383 + 0.014775 \cdot \lg(6 \cdot 10^{-5} \cdot 10^{-7.36 \cdot 4} / 55.3^6) = 0.73 \text{ Volts.}$$

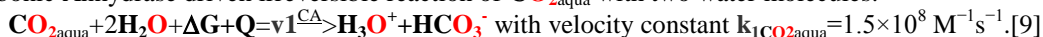
Oxidative stress potential decreases about $\Delta E_{O_{2aq}} = E_{O_2} - E^{\circ}_{O_2} = 0.73 - 1.382 = -0.652 \text{ Volts}$ Potential minimizes Free energy content for oxygen about -251.6 kJ/mol :

$$\Delta G_{O_{2aq}} = \Delta E_{O_{2aq}} \cdot F \cdot n = -0.652 \cdot 96485 \cdot 4 / 1000 = -251.6 \text{ kJ/mol.}$$

Strong oxidant $G_{O_2} = 237.191 \text{ kJ/mol}$ becomes fire safe for Biochemistry with free energy $G_{O_{2aq}} = 12,17 \text{ kJ/mol}$.

1.1.2. Synthesis of Carbonic Anhydrase CA indispensable Attractor.

Carbonic Anhydrase driven irreversible reaction of CO₂aq with two water molecules:



Neutralization $H_3O^+ + HCO_3^- <=^{CA}> CO_{2aq} + 2H_2O$ velocity constant is: $k_2 = 5.16885 \cdot 10^{18} \text{ M}^{-2} \text{ s}^{-1}$.

Equilibrium constant have to calculate in the velocity constants ratio expression:

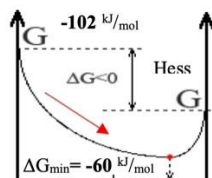
$$K_{eqCA} = k_{ICo_{2aq}} / k_2 = \frac{[HCO_3^-]_{aq} [H_3O^+]_{aq}}{[CO_2]_{aq} [H_2O]^2} = K_a / [H_2O]^2 = 10^{-7.0512} / 55.3^2 = 2.906 \cdot 10^{-11}.$$

Bicarbonate buffer system acid protolysis constant $pK_a = 7.0512$ is friendly to pH=7.36:

Original $pK_{a,CO_{2aq}} = 7.0512$ obtained and calculate for **BUFFER solution**. [1] Carbonic Anhydrase synthesis solve for bioenergetic perfect order homeostasis as Self-Organization Attractor. [3,4]

Neutralization reaction Hess Free energy is: $\Delta G_{Hess} = 2\Delta G^{\circ}_{H_2O} + \Delta G^{\circ}_{CO_2} - \Delta G^{\circ}_{H_3O^+} - \Delta G^{\circ}_{HCO_3^-} = -102 \text{ kJ/mol}$.

Free energy change minimum expression is negative: $\Delta G_{eq} = -R \cdot T \cdot \ln(1/K_{eqCA}) = -60 \text{ kJ/mol}$.



Reactant H₃O⁺+HCO₃⁻ A+B 50 % C+2D products CO₂aq+2H₂O.

Figure 2. Exothermic and exoergic neutralization Hess Free energy change $\Delta G_{neutralization}$ negative -102 kJ/mol , but minimizes -60 kJ/mol reaching equilibrium mixture : $1/K_{eqCA} = K_{eq} = 34459000000$ at presence of Carbonic Anhydrase.

1.1.3. Multipurpose Self-Organization Attractor pH=7.36 creates positive , negative charged groups:

R-COO⁻, R-NH₃⁺, HPO₄²⁻, R-PO₄²⁻, HCO₃⁻ as free and linked in R molecules: amino acids, proteins, nucleic acids, carbohydrates, coenzymes.

Buffer systems in the Life organism trend to Self-Organization Attractor pH value 7.36. Each of dominate buffer system have 7.36 friendly maximum (Figure 3. and 4.) of the buffer capacity: dihydrogen phosphate $pK_{a-H_2PO_4}=7.199$ [1] and Carbonic Anhydrase create protolysis calculate constant: $pK_{a-CO_2aqua}=7.0512$. [1]

Proteins as long chain polypeptides and free amino acids with four type acid groups constitute 47 values for classic acid protolysis constants. In three forms pK_{a-COOH} , $pK_{a-NH_3^+}$, $pK_{aRgroup}$: for deprotonate carboxylate negative anion $R-COO^-$, for protonate positive charged ammonium cation $R-NH_3^+$, neutral phenolic acid Tyr- OH and Cys- SH neutral sulfhydryl groups. [6]

1.1.4. Shuttle hemoglobin stabilized multipurpose Self-Organization Attractor pH=7.36.

Hemoglobin in tissue desorbs oxygen O_{2aqua} for exchange to HCO_3^- and H^+ but in lungs releases HCO_3^- and H^+ due to adsorption of oxygen O_{2aqua} . [6] Exchange equilibrium depends on oxygen concentration in arterial $6 \cdot 10^{-5}$ M and venous $0.426 \cdot 10^{-5}$ M according actual hemoglobin sensitive equilibrium to [oxygen concentration in blood](#): [6]

$O_{2aqua} + (H^+ His63,58)Hb_T...salt\ bridges...(HCO_3^-) + H_2O \rightleftharpoons Hb_R(O_2) + H_3O^+ + HCO_3^-$:
arterial $[O_{2aqua}] = 6 \cdot 10^{-5}$ M, fraction $[(H^+)Hb_T...salt\ bridges...(HCO_3^-)] = 0.04$, fraction $[Hb_R(O_2)] = 0.96$, [6]
venous $[O_{2aqua}] = 0.426 \cdot 10^{-5}$ M, fraction $[(H^+)Hb_T...salt\ bridges...(HCO_3^-)] = 0.37$, fraction $[Hb_R(O_2)] = 0.63$. [6]

In one blood circulation organism consume $0.96 - 0.63 = 0.33$ fraction of oxygen from arterial saturated fraction $0.96 = [Hb_R(O_2)]$. [6] Stabilized Norma concentrations $[HCO_3^-] = 0.0154$ M, $[CO_{2aqua}] = 0.0076$ M sustain Self-Organization Attractor pH=7.36. Henderson Haselbalh expression for Brensted protolysis calculates Attractor value 7.36: $pH = pK_a + \log \log \left(\frac{[HCO_3^-]}{[CO_{2aqua}]} \right) = 7.0512 + \log(0.0154 \text{ M} / 0.0076 \text{ M}) = 7.36$.

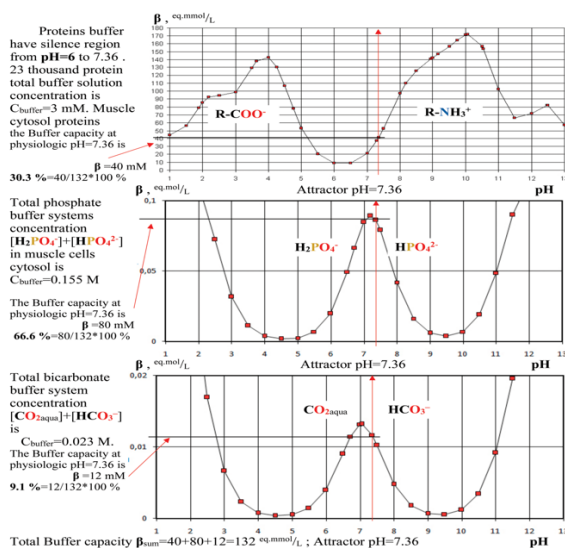


Figure 3. Cytosol muscle cells. Buffer capacities versus pH values from 1 to 13. Actual buffer capacity at Attractor pH=7.36 for two dominate phosphate, bicarbonate and total protein made buffer.

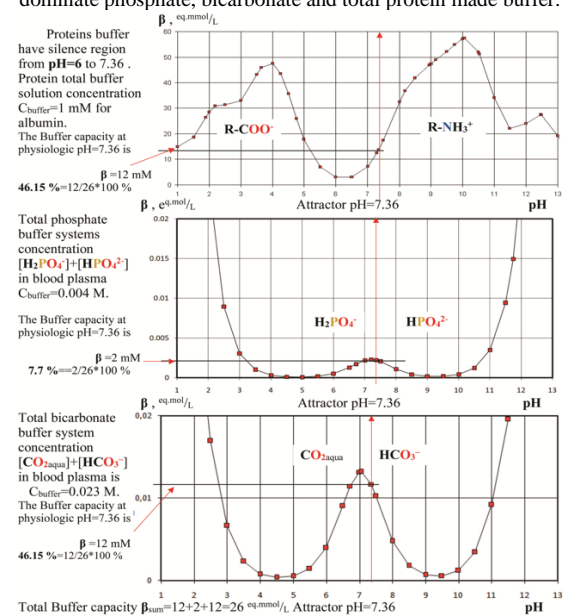


Figure 4. Extra Cellular space Blood plasma. Buffer capacities versus pH values from 1 to 13. Actual buffer capacity at Attractor pH=7.36 for two dominate phosphate, bicarbonate and total protein made buffer.

Buffer capacity is acid Δn_{ac} or base Δn_b equivalent_mols/ in one Liter changing pH per one unit $\Delta pH = \pm 1$.

Three type buffer systems create multipurpose Self-Organized Attractor pH=7.36 for perfect homeostasis order with charged groups as free and linked in molecules R . 11th and 12th pages: [BUFFER solution](#). [1]

1.1.5. The primary Self-Organization Attractor air oxygen O_2 20.95 %.

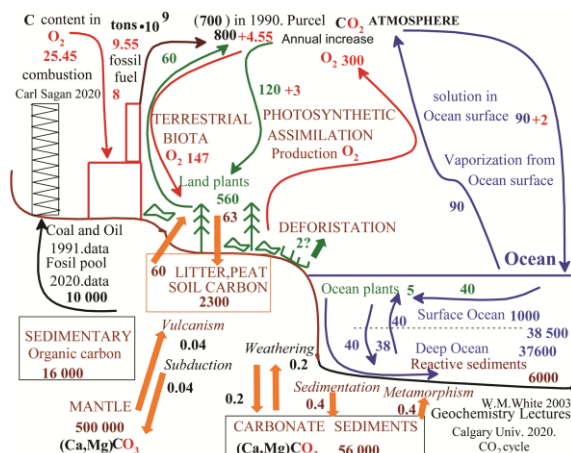


Figure 5. CO_2 in atmosphere last thirty Years. CO_2 and O_2 cycle combined data from: 1991st Kotz JC, Purcell KF 700 Gt of CO_2 in atmosphere [10], 2003rd White VM 725 Gt of CO_2 [11] and 2020th Carbon cycle University Calgary 800 Gt of CO_2 in atmosphere. [12]

Civilization with regular pollutions add about 1.2 % to atmosphere annual 4.55 Gt to reach 800 Gt $CO_2 \uparrow_{gas}$ in 2020th global and cosmic processes oscillation see on Figure 6. for 600 million Years.

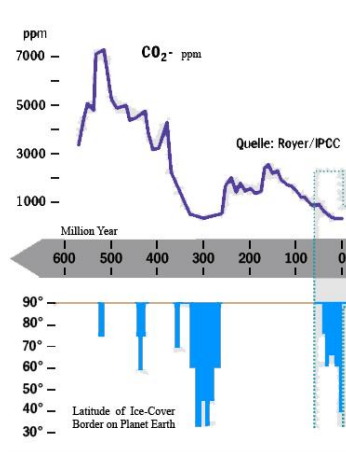


Figure 6. Climate reconstruction history since 600 Million Years ago: Atmospheric CO_2 content in units' ppm, Earth ice Cover Border Latitude and temperature oscillation from -50° C to 45° C degrees. [13]

The Carbonic Anhydrase and photosynthesis restore and maintain primary Self-Organization Attractor oxygen O_2 level 20.95 % during 500 million Years. [1,6,13]

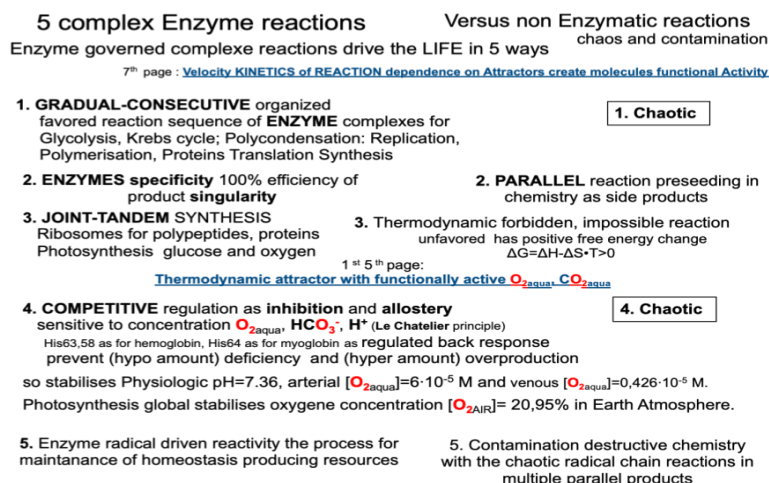


Figure 7. Self-Organization Attractors claim order versus non-enzymatic reactions chaos and contamination.

Five type complex reactions in enzyme clusters.

Self-Organization Attractors sustain the functional activity perfect order for homeostasis.

Deviation from Attractor values create homeostasis disorder as Chaos.

1.1.6. Results and Conclusions Summary

Self-Organization Attractors create perfect order homeostasis link Bioenergetic.

Self-Organization Attractors create functional active molecules reactivity order for homeostasis and bioenergetic. The order of functionally active molecules drives homeostasis under rule Attractors. Reaching of Attractor values create homeostasis order out of disorder. Chaos disorder homeostasis. The molecules functional activation of oxygen O_{2aq} and of carbon dioxide CO_{2aq} initiates as **Self-Organization** Attractors. Attractors are two types and multipurpose: the primary Attractors common for Biosphere, the secondary Attractors for individual organisms and multipurpose pH=7.36, water, air oxygen.

Oxygen O_{2aq} decreased power for functional active isoxia Norma solution in blood so in cytosol too driven with four Attractors: water triplet state of oxygen, water concentration $[H_2O] = 55.3 \text{ mol/Liter}$, air oxygen level 20.95 % for five hundred million Years, pH=7.36 for the concentration $[H_3O^+] = 10^{-7.36}$ M.

CA Carbonic Anhydrase work as primary Attractor for Biosphere which forms dominate bicarbonate buffer of CO_{2aq} acid protolysis constant $pK_a = 7.0512$. Henderson Haselbalh expression calculates Attractor value 7.36, which corresponds to concentration $[H_3O^+]$. Attractor 7.36 creates functional activity of molecules with charged groups negative, positive: HPO_4^{2-} , HCO_3^- , $R-COO^-$, $R-NH_3^+$, $R-PO_4^{2-}$ as free and linked in amino acids, proteins, nucleic acids, carbohydrates, coenzymes, **R** molecules. Carbonic Anhydrase synthesis solve perfect order of homeostasis and bioenergetic as Self-Organization Attractor. [3,4]

The Attractors values in organism compartments dissipative structures drive the perfect homeostasis order with enzymes clusters on five type complex reactions. Order is key for surviving of organism. Deviation from Attractor values cause loss the homeostasis order of functional activity. Chaotic reactions waste the resources and stop the homeostasis, the non-equilibrium complex processes. The homeostasis becomes extinct from Biosphere.

Attractors are indispensable to form functionally active molecules for perfect order homeostasis and bioenergetic reactions. Attractors destiny is irreversible free energy change $\Delta G_{\text{Homeostasis}}$ transduction between functional active molecules. Note: Homeostasis trend to equilibrium but never reaching because it is non-equilibrium state.

1.1.7. Acknowledgements.

The author would like to acknowledge all the contributions of the field "Prigogine thermodynamic Attractors drive homeostasis with functionally activate O_{2aq} , CO_{2aq} " which critically appreciate this study:

Thanks for critical discussions with MD Aivar Grinberg about Attractors in Biochemistry to see indispensability for Life create functionally activate molecules to maintain the homeostasis of organisms.

Thanks for Riga Stradin's University Library about supporting literature studies.

Thanks for Riga Stradin's University department staff of Human Physiology and Biochemistry who supporting may advanced studies in Biochemistry of Prigogine Thermodynamic Attractors.

1.1.8. References.

1. David R. Lide. CRC Handbook of Chemistry and Physics .90th ed. Taylor and Francis Group LLC; 2010 .
2. Prigogine I, Defey R. Chemical Thermodynamics. Longmans Green & co ©; 1954.
3. Prigogine I, Nicolis G. Self-Organization in Non-Equilibrium Systems. Wiley, 1977.
4. Prigogine I. Time, Structure and Fluctuations. Lecture, The Nobel Praise in Chemistry; 1977.

5. Kuman M. New light on the attractors creating order out of the chaos. *Int J Complement Alt Med.* **11**(6), 337, (2018) ;
6. Nelson DL, Cox MM. Lehninger Principles of Biochemistry. 5th ed. New York: W.H. Freeman and company; 2008.
7. Xing W, Yin G, Zhang J. Rotating Electrode Method and Oxygen Reduction Electrocatalysts. *Elsevier*; 6 (2014) .
8. Alberty RA. Biochemical Thermodynamic's : Applications of Mathematics. John Wiley & Sons, Inc. 1-463, (2006).
9. Pinard MA, Mahon B, McKenna R. Probing the Surface of Human Carbonic Anhydrase for Clues towards the Design of Isoform Specific Inhibitors. *BioMed Research International*; **2015**, 3 (2015).
10. Kotz JC, Purcell KF. Chemistry and chemical reactivity. Saunders College Publishing; 1991.
11. White VM. THE CARBON CYCLE, ISOTOPES, AND CLIMATE I and II. Lectures 37, 38; 2003 .
12. Hanania J, Pomerantz C, Stenhouse K, Toor J, Donev J. Carbon cycle. University of Calgary's 2020 .
13. Der wohltemperierte Planet. *Der Spiegel*. 2007 Nr.19:148-154. German .

GAS SEPARATION PROPERTIES OF MIXED MATRIX MEMBRANES PREPARED WITH GRAPHENE OXIDE

Sevgi CANCA¹, Sennur DENİZ²,

^{1,2} Yıldız Technical University, Faculty of Chemical and Metallurgical Engineering,
Chemical Engineering Department, 34220, Esenler, Istanbul-Turkey

e-mail: f2020058@std.yildiz.edu.tr; deniz@yildiz.edu.tr

Abstract

In this study, we used PEBA and PI as a monomer in synthesis of polymer membrane while the modification agent is GO. PEBA/GO and PI/GO mixed matrix membranes were prepared by adding graphene oxide (GO) dopant at % 0-0.1-0.2-0.3 percent by weight to PEBA and PI polymer solution. Polymer membranes prepared by solution casting method. The gas permeability and selectivity of modified polymer membranes were tested. The gas separation experiments of the membranes were performed at 35 °C and 3 bar feed pressure. The main aim of this study is to increase the selectivity and permeability of membranes in gas separation applications.

Key Words: Gas separation, Mixed matrix membranes, Poly(ether-b-amide), Polyimide, Graphene Oxide

1. Introduction

Membrane-based gas separation technology is a separation process which allows certain species to pass through the membrane while restricting the others depending on the properties of the membrane material. Membrane technology is commonly used for industrial applications such as air separation, ammonia production, carbon dioxide separation, nitrogen generation and hydrogen recovery. The advantages of this technology over traditional separation processes include lower capital and operating costs, better efficiency, and lower risk.

Hydrogen is seen as the energy carrier of the future with its high energy density and environmentally friendly features. Hydrogen, which is not found in pure form in nature, can be separated from the gas mixture by various techniques. Gas mixtures are separated in industrial systems using cryogenic distillation, adsorption and polymeric membranes. The most important parameters emphasized when examining the efficiency of membrane systems are selectivity and permeability. Permeability and selectivity are the key parameters for evaluating the separation performance of a membrane. Permeability reflects the rates at which components (penetrants) are transported through a membrane, and selectivity is the ratio of the permeability of the more permeable component to the less permeable one. Both high selectivity and high permeability are required for an effective gas separation system [1].

A new approach, mixed matrix membranes (MMMs), are mixed matrix materials consisting of homogeneously intertwined polymeric and inorganic particle matrices. Metal-organic frameworks (MOFs) have attracted attention due to their unique properties in terms of low density, high porosity and high surface areas, especially for their superior potential in gas storage and gas separation applications. Various types of MOFs can be synthesized by varying the combination of different organic binders and metal ions. This adaptability makes MOFs promising candidates for separation applications compared to zeolites and other inorganic fillers. The selection of suitable MOF/polymer pairs is crucial for experimental efforts to improve the performance of MMMs. The aim of this study is to develop a mixed matrix membrane with different polymeric bases of poly(ether-b-amide) (PEBA) and Polyimide (PI) containing graphene oxide (GO) as inorganic filler for hydrogen separation. Matrimid[®] 5218 is a commercially available thermoplastic PI.

2. Experimental

2.1. Materials

Poly(ether-b-amide); PEBAX[®] 1657, ethanol (C₂H₅OH), Matrimid[®] 5218 (PI) polymer was purchased from Huntsman Corporation (USA). The solvent for polyimide was N-methyl-2-pyrrolidone (NMP, 99% VWR Chemicals). Graphene oxide (GO) was supplied by AEROFEN (TR).

2.2. Methods

Preparation of nanocomposite (PEBA/GO): The PEBA/GO MMMs were fabricated by a solution casting method. PEBA were dispersed in a solvent mixture of 70 wt % ethanol and 30 wt % water and GO powders were dispersed in a solvent mixture of 70 wt % ethanol and 30 wt % water and then treated by ultrasonication for 1 h. After that a homogeneous solution was obtained by mixing these two solutions. Then the obtained uniform

suspension, poured into a petri dish. After solvent evaporation at room temperature, the petri dish was placed in a vacuum.

Preparation of nanocomposite (PI/GO): The PI/GO MMMs were fabricated by a solution casting method. For the preparation of the dope solution (10 wt% of solid), first of all, the desired amount of GO (to obtain 0.1, 0.2 and 0.3 wt% of GO in MMM) was dispersed into NMP and the mixture was stirred at room temperature and sonicated. Then, the polymer was added into the GO solution. A petri dish was used for solution casting. After solvent evaporation at room temperature, the petri dish was placed in a vacuum.

2.2. Gas permeation properties

Gas permeability coefficients of membranes were calculated by using a constant volume-variable pressure gas permeability device. Permeability measurements were performed according to the steady-state method at 35 °C. In this study, single gases (H₂, N₂, CO₂, and CH₄) were used to measure gas separation performances of membranes. The circularly cut test specimens used in permeability tests were masked with a self-adhesive aluminum foil. And the vacuum pump were used. The membrane was sealed and tightened. The gas pressure fed to the system was kept constant at 3 ± 0.2 bar. Gas was fed to the system by a valve in the upper part of the cell and the pressure change in the lower part was recorded with the data recording program.

The gas permeation of polymeric membranes is described by the solution–diffusion model [2]. The gas transport occurs when the gas molecules are dissolved in the membrane surface, and molecules diffuse across the membrane by way of the cavities present in the polymer. The permeability results from the contribution of these two mechanisms, and can be described by Equation (1):

$$P = D \times S \quad (1)$$

where P is the permeability of membrane in Barrer (1Barrer = $1 \times 10^{-10} \text{ cm}^3 \text{ (STP)-cm/cm}^2 \text{ s cmHg}$), D is the diffusion coefficient, and S is the sorption coefficient.

Typically, the selectivity (α) is defined as the relation of the permeability for the components A and B. Ideal selectivity, $\alpha_{A/B}$, is the ratio of individual permeability coefficients for the gas pairs. The general selectivity of a material defined in Equation (2) is a function of diffusivity (D_A/D_B) and selectivity ratios (S_A/S_B).

$$\alpha_{A/B} = \frac{P_A}{P_B} = \frac{D_A}{D_B} \times \frac{S_A}{S_B} \quad (2)$$

3. Results of discussion

3.1. Gas Permeability and Selectivity

Table 1. PEBA/GO Results of Gas Permeability and Selectivity

| Membrane | Permeability, P (Barrer*) | | | | | Ideal Selectivity, α | | | |
|-------------|---------------------------|----------------|----------------|----------------|-----------------|-----------------------------|------------------------------|---------------------------------|--|
| | N ₂ | H ₂ | C | C | H ₂ | H ₂ | CO | C | |
| | | | H ₄ | O ₂ | /N ₂ | /CH ₄ | ₂ /N ₂ | O ₂ /CH ₄ | |
| PEBA | 1.2114 | 12.5958 | 4.2467 | 39.8120 | 10.977 | 2.9660 | 32.8644 | 9.3748 | |
| PEBA/GO-0.1 | 1.2362 | 13.8670 | 4.5840 | 34.1599 | 11.2174 | 3.0252 | 27.6329 | 7.4519 | |
| PEBA/GO-0.2 | 1.2396 | 5.680 | 3.0910 | 22.0202 | 4.1691 | 1.6719 | 17.7639 | 7.1239 | |
| PEBA/GO-0.3 | 1.1124 | 4.6849 | 2.7396 | 21.4582 | 4.2115 | 1.7101 | 21.0879 | 8.5626 | |

Table 1. PI/GO Results of Gas Permeability and Selectivity

| Membrane | Permeability, P (Barrer*) | | | | | Ideal Selectivity, α | | | |
|-----------|---------------------------|----------------|----------------|----------------|-----------------|-----------------------------|------------------------------|---------------------------------|--|
| | N ₂ | H ₂ | C | C | H ₂ | H ₂ | CO | C | |
| | | | H ₄ | O ₂ | /N ₂ | /CH ₄ | ₂ /N ₂ | O ₂ /CH ₄ | |
| PI | 0.3946 | 6.7232 | 0.257 | 1.4603 | 17.0380 | 20.0642 | 3.7007 | 4.4836 | |
| PI/GO-0.1 | 1.0003 | 7.0213 | 0.3432 | 1.3275 | 7.0192 | 20.4583 | 3.8680 | 3.8680 | |
| PI/GO-0.2 | 1.5751 | 6.0123 | 0.4874 | 0.8545 | 3.8171 | 12.3354 | 0.5425 | 1.7532 | |
| PI/GO-0.3 | 1.6671 | 4.5479 | 0.6649 | 0.6600 | 2.7281 | 6.8399 | 0.3958 | - | |

4. CONCLUSION

PEBA/GO and PI/GO mixed matrix membranes were prepared by the adding 0.1; 0.2 and 0.3 wt.% of graphene oxide (GO) in PEBA and PI polymer matrix with solution-casting method. All membranes were prepared with good stability for gas permeation tests. The gas permeability measurements of MMMs were performed at 35 °C and 3 bar feed pressure for H₂, N₂, CH₄, and CO₂ gases. H₂/N₂ and CO₂/N₂ selectivities of membranes was determined by time-lag method. For the PEBA/GO-0.1 membrane, it was found that the higher selectivity values were measured. For the PI/GO-0.1 membrane it was found that the higher selectivity values were measured. In the continuation of this study, PEBA/GO@MOF and PI/GO@MOF MMMs will be prepared and performed the gas permeability measurements for the enhancing of selectivity values.

References (Times New Roman, 10pt, Bold)

- [1] P.S. Goh, A.F. Ismail, S.M. Sanip, B.C. Ng, M. Aziz, (2011), Recent advances of inorganic fillers in mixed matrix membrane for gas separation, *Separation and Purification Technology*, 81 243-264.
- [2] Castro-Muñoz, Roberto and Fila, Vlastimil, (2018), Progress on Incorporating Zeolites in Matrimid®5218 Mixed Matrix Membranes towards Gas Separation, *Membranes*, 8, 2077-0375